AMSI SUMMER RESEARCH SCHOLARSHIPS 2023–24

SET YOUR SIGHTS ON RESEARCH THIS SUMMER

Modelling impact resistant materials for use in protective gear

Minh Thu Nguyen
Supervised by Dr. Louise Olsen-Kettle
Swinburne University of Technology

AMSI AUSTRALIAN MATHEMATICAL SCIENCES INSTITUTE

Abstract

Advancements in material science and engineering have spurred innovations in the design of hierarchical structures, offering promising solutions for enhancing mechanical properties and energy absorption in various applications. This paper delves into the mechanical properties and energy absorption capabilities of hierarchical structures, focusing on ceramic materials as a model. Drawing inspiration from Sierpinski triangles and hexagrams, we explored the impact of hierarchical design on the response of structures under quasi-static compression. By implementing a methodology that involves digitizing curves, creating meshes with Gmsh, and conducting finite element simulations using Esys-Escript, we analyzed stress-strain curves and calculated key performance metrics. Our findings revealed that hierarchical structures exhibit a two-stage failure mechanism, enhancing ductility and providing warning signs before complete collapse. Also, in structures composed of only one type of triangle, as the size of each triangle increases, the energy absorption capacity of the structure decreases. The study emphasises the significance of hierarchy in improving the mechanical performance of materials, with potential applications in protective gear and structural engineering. Future research avenues may involve optimisation strategies to maximise ductility and energy absorption efficiency in hierarchical structures.

{ hierarchical structures, mechanical properties, energy absorption materials, finite element simulations}

1 Introduction

In the realm of protective gear, the concept of energy absorption stands as a cornerstone in safeguarding individuals from injury during impact events (Fernandes et al. 2019). Picture a scenario where a motorcyclist wearing a helmet collides with another vehicle. During impact, kinetic energy from the moving motorcycle is transferred to the rider's head. However, the helmet's design is engineered to absorb this energy. Through the helmet's outer shell and inner padding, kinetic energy is distributed and cushioned, mitigating the severity of potential head injuries (Daneshvar et al. 2011). This fundamental process underscores the importance of energy absorption in minimizing trauma and ensuring the safety of individuals during accidents.

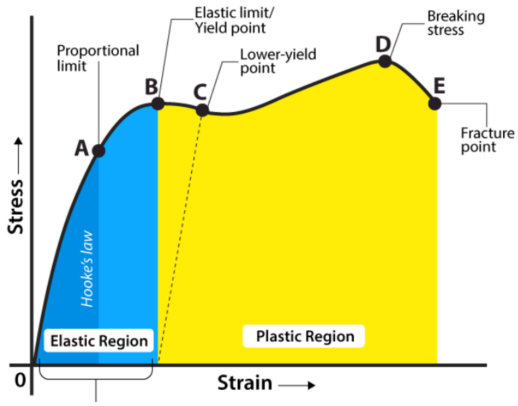

Figure 1: A typical stress-strain curve (Velling 2020)

Energy absorption, a fundamental concept in the realm of protective gear, refers to the ability of materials

to dissipate kinetic energy upon impact (Lu 2003), thereby reducing the force transmitted to the wearer's body. Referring to Figure 1, a typical stress-strain curve provides valuable insights into the energy absorption process. Initially, as stress is applied to the material, it undergoes elastic deformation, characterised by a linear relationship between stress and strain. This elastic modulus region represents the material's ability to absorb energy elastically, allowing it to return to its original shape once the force is removed. However, as stress exceeds the material's yield point, plastic deformation occurs, marking the onset of energy absorption through permanent deformation. Yield stress, a critical parameter in energy absorption, signifies this transition. As stress continues to increase, the material may undergo further deformation until reaching ultimate compressive strength, where it ultimately fractures. Fracture toughness becomes crucial here, indicating the material's ability to resist crack propagation and absorb energy effectively (Taylor 2018).

Building upon the foundational research of Qian Cheng and team (Cheng et al. 2023), our project explores the performance of ceramic composite materials in terms of energy absorption capabilities. While previous studies focused on thermoplastic urethane and Sierpinski triangles, our research diverges by modeling alumina, a brittle material.

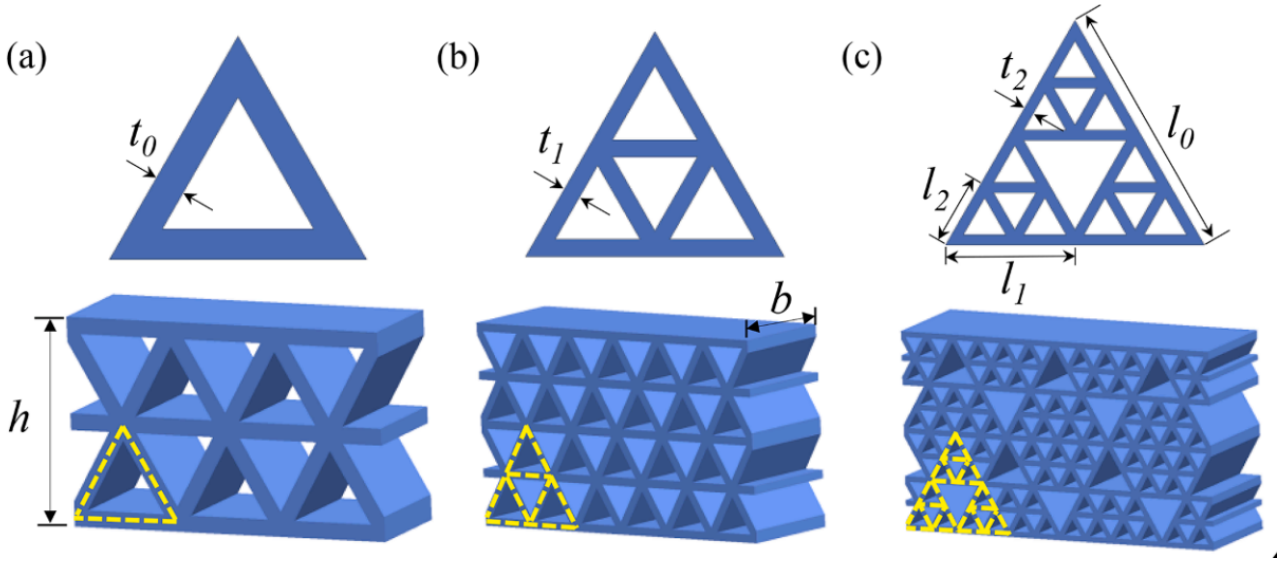

Figure 2: Schematics of hierarchical composites and their unit cells composed of Sierpinski triangles with different hierarchy orders. (a) Zero-order structure: HTC-0, (b) First-order structure: HTC-1, and (c) Second-order structure: HTC-2.

Cheng et al. conducted in-plane compressive tests on hierarchical cellular structures (HTCs) using an electronic universal testing machine. They observed typical stress-strain responses characterised by linear elasticity, stress plateau, and densification regimes. HTC-1 and HTC-2 displayed similar behavior in the linear elastic regime but diverged notably in the stress plateau. HTC-2 exhibited a longer elastic regime, higher initial peak stress ($\sigma_{\max}$), and fluctuations in the stress plateau, indicative of localised collapsing. They further investigated the mechanical behavior of HTC-2 through digital camera recordings and numerical simulations using LSDYNA. Simulation models involved a constant loading speed with constrained out-of-plane motion

and defined contact conditions between the rigid plate and HTCs. Performance indexes including densification strain, initial peak stress, mean plateau stress, and energy absorption were quantitatively evaluated, revealing distinct mechanical performances among HTCs, particularly notable enhancements in HTC-2 compared to HTC-1.

In this paper, we digitise and analyse curves for HTC-1 and HTC-2 to validate Cheng et al.'s findings. Subsequently, we meticulously review and expand upon the Python code to suit our research goals, generating scripts for Gmsh files—an essential tool for creating complex shapes and meshes for simulations. The meshes are then inputted into finite element software, specifically Esys-Escript, facilitating stress-strain analyses on various triangular composite structures. This approach enables the evaluation of mechanical performance and energy absorption capabilities, with results reported in terms of densification strain, initial peak stress, and energy absorption. Densification strain refers to the extent of plastic deformation beyond the yield point, while initial peak stress refers to the highest stress a material experiences in the early stages of deformation (Lu 2003). Meanwhile, energy absorption refers to the material's capacity to dissipate kinetic energy during deformation or impact (Lu 2003).

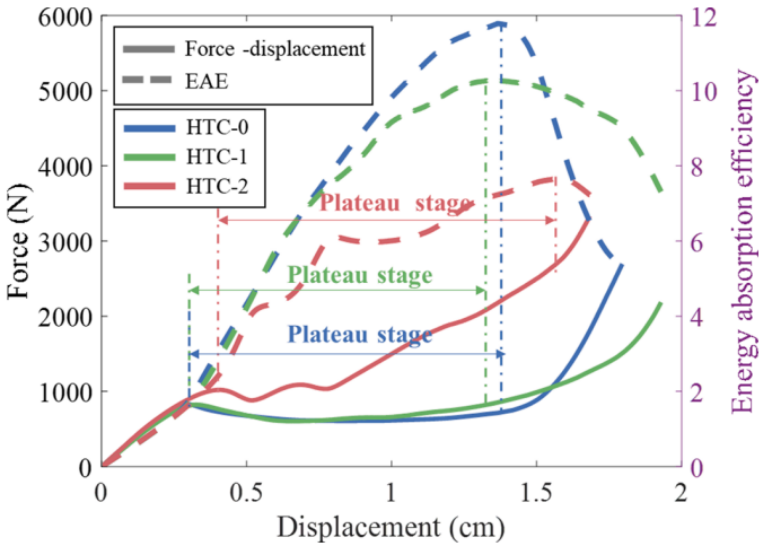

Figure 3: Force-displacement curves (solid lines) and corresponding energy absorption efficiency curves (dashed lines) of the three HTC structures under quasi-static loading. The plateau stage leading to densification for each HTC is marked between the end of the linear elastic region and the peak of the corresponding energy absorption efficiency curve.

Gmsh is an open-source finite element mesh generator software, widely used for creating three-dimensional computational meshes (Geuzaine & Remacle 2009). In this paper, Gmsh is utilised to create intricate geometric shapes and generate meshes for simulations, facilitating the accurate representation of hierarchical structures in the project.

Esys-EScript is an open-source software package designed for the numerical simulation of coupled, multi-physics problems using the finite element method (Schaa et al. 2016, Gross et al. 2007). It provides a Python interface for creating and solving finite element models, making it particularly useful for researchers and engi-

neers working in geophysics, mechanics, and other related fields. In this work, Esys-EScript is used to model and simulate the mechanical behavior of hierarchical structures, allowing for the analysis of energy absorption properties under different loading conditions.

Simulation of compressive loads using esys-escript

We, now, delve into the mechanics of how esys-escript operates to simulate compressive loads and analyze ensuing damage evolution within materials. To achieve this, we first discuss the iterative process employed by esys-escript, where in each loading step, it calculates the new displacement vector while considering the applied load and boundary conditions (Mondal et al. 2020*a*,*b*). Furthermore, esys-escript assesses the resulting damage to the material using a strain-based failure criterion and a damage evolution law. Material properties are then updated based on the extent of damage before applying the next loading step, ensuring an accurate representation of the material's response to compression. Utilizing the Finite Element Method (FEM) with linear tetrahedron elements, implemented in esys-escript (Olsen-Kettle et al. 2022), we solve the momentum equation for the displacement vector.

Table 1: Parameters in damage evolution law and material properties for alumina

Parameter	**Value**
Young's modulus (GPa)	314
Poisson's ratio	0.21
γ	4.5
E (MPa)	215–413
ν	0.333
σ_c (MPa)	690–5500
σ_t (MPa)	350–665

Our goal is to solve the 3D elastostatic equilibrium equations under quasi-static displacement loading. To ensure equilibrium within the system, we rely on the conservation of momentum equation, expressed in Einstein notation as:

$$\sigma_{ij,j} = 0 \tag{1}$$

Here, σ denotes the stress tensor, and the lower index j indicates the derivative concerning spatial direction x_j.

In the context of isotropic, linear elasticity, the stress tensor components (σ_{ij}) are dictated by Hooke's law:

$$\sigma_{ij} = C_{ijkl}.\varepsilon_{kl} \tag{2}$$

where ε_{kl} represents the strain tensor.

$$C_{ijkl} = \frac{E\nu}{(1+\nu)(1-2\nu)}\delta_{ij}\delta_{kl} + \frac{E}{2(1+\nu)}(\delta_{ik}\delta_{jl} + \delta_{il}\delta_{jk}) \tag{3}$$

Here, E denotes Young's modulus, ν stands for Poisson's ratio, and δ_{ij} is the Kronecker delta symbol.

Expressed in geometrical linearized form, the strain tensor (ε_{kl}) is given by:

$$\varepsilon_{kl} = \frac{1}{2}(u_{k,l} + u_{l,k}) \tag{4}$$

Here, u represents the displacement vector.

Our damage model operates based on a strain-based failure criterion, employing a scalar equivalent strain $\tilde{\varepsilon}$ (Peerlings et al. 2000). This equivalent strain, based on the von-Mises stress and Hooke's law and used to evaluate the initiation and progression of damage within the material, is expressed as:

$$\tilde{\varepsilon} = \frac{\gamma - 1}{2\gamma(1 - 2\nu)} I_1 + \frac{1}{2\gamma}\sqrt{(\gamma - 1)^2(1 - 2\nu)^2 I_2 - 12\gamma(1 + \nu)^2 J_2} \tag{5}$$

Here, I_1 represents the first invariant of the strain tensor, and J_2 denotes the second invariant of the deviatoric strain tensor.

As damage progresses, the elastic Young's modulus (E) is altered, as indicated by the equation:

$$E = E_0(1 - D) \tag{6}$$

In this equation, E_0 signifies the Young's modulus prior to loading, while D represents the scalar damage variable, ranging from 0 (undamaged) to 1 (complete loss of material coherence).

In our damage evolution model, the evolution of the damage variable D is governed by the threshold variable κ, with the update of κ defined by specific conditions. Additionally, the material's elastic modulus (E) undergoes reduction according to a power law function, with specific parameters influencing the rate and extent of damage growth. The isotropic damage model (Mondal 2019, Mondal et al. 2019, Olsen-Kettle et al. 2022) was employed, where the elastic Young's modulus (E) was reduced as damage progressed, with the scalar damage variable D describing the material's state.

Figure 4 illustrates five geometric configurations of the structures analyzed in our study. The Sierpinski-inspired triangle structure features a fractal pattern characterised by repeating triangular elements at three different hierarchical levels, forming a self-similar pattern, while the Hexagram structure is also using Sierpinski triangles with only two levels of hierarchy to form hexagram shapes. The H2H3 structure considers a regular array of alternating H2 and H3 triangles, while the H2-only and H3-only structures focus solely on either H2 or H3 triangles. Leveraging advanced software tools like esys-escript and Gmsh, we seek to optimise and validate our models to contribute to the development of more effective protective gear.

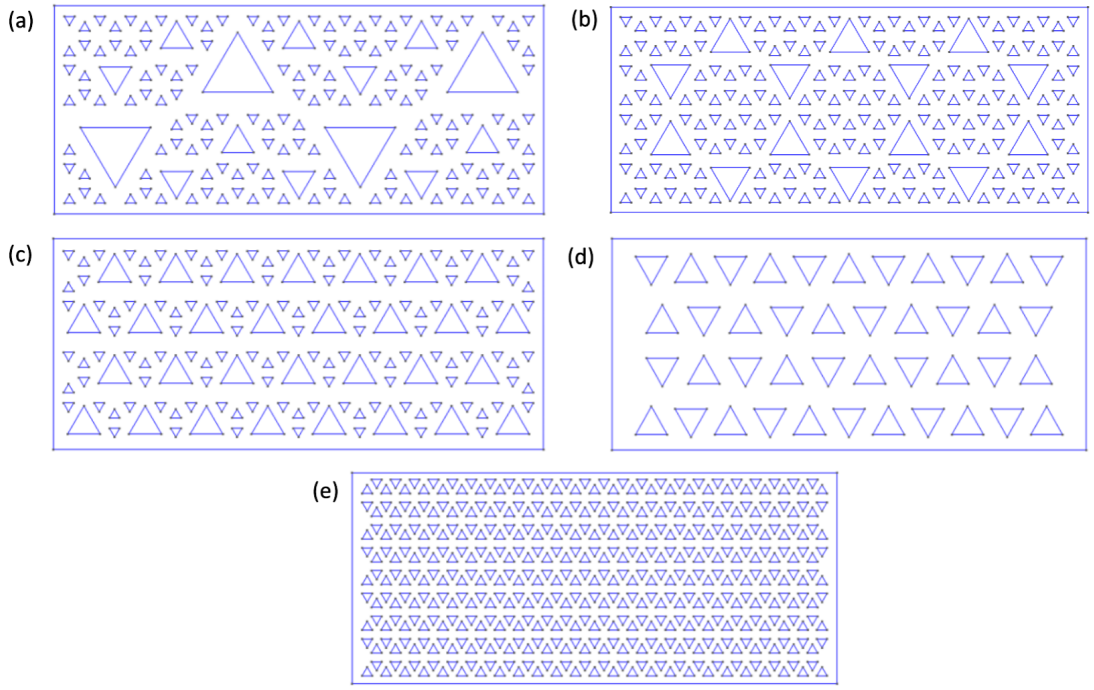

Figure 4: Five different geometric configurations of the structures analyzed in our study, with (a) Sierpinski-inspired - Fractal, (b) Hexagram, (c) H2H3, (d) H2, (e) H3. All designs maintain identical surface area, volume, and loading surface area for comparative analysis.

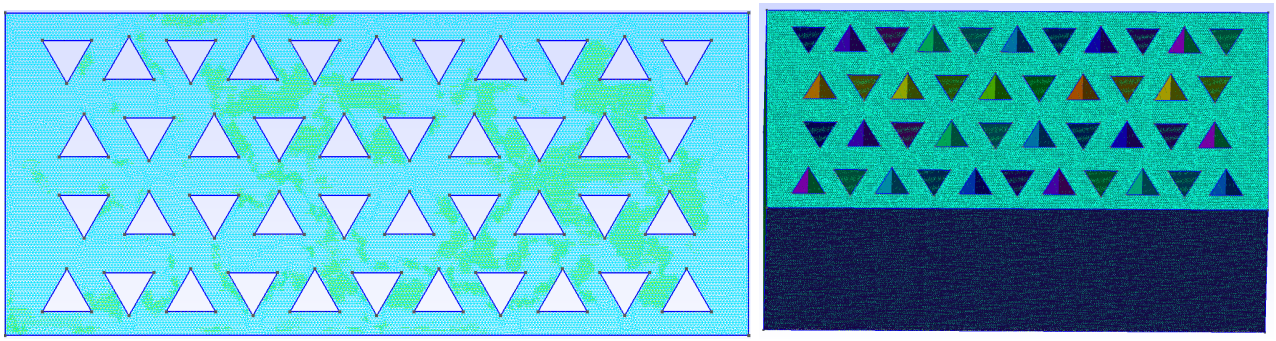

(a) H2 in 2D mesh

(b) H2 in 3D mesh

Figure 5: H2 structure shown in gmsh

It is important to consider the limitations of the 3D printer when designing and printing structures for testing. One significant constraint is the minimum distance requirement between any two elements, which typically stands at 2 millimeters (Wang et al. 2020). Adherence to printer specifications is crucial, with particular attention to minimum and maximum sizes within the design. For instance, the minimum wall thickness is dictated by the nozzle diameter, set at 0.4 mm (F. P. Bos & Salet 2019). However, for optimal print quality, a double wall thickness is recommended, resulting in a maximum outer diameter that is 1.6 mm less than the

maximum length of 50 mm, allowing space for the surrounding box. When these constraints are not followed, issues with printing quality and structural integrity may arise, as illustrated in figure 5 depicting a 3D-printed structure that failed to adhere to the printer constraints. Resolution limitations also impact the printing process, underscoring the importance of meticulous design considerations and adherence to printer specifications.

Figure 6: An issue we encountered when initially not following 3D-printer constraints.

Table 2: Geometrical parameters for hierarchical tubes shown in Figure 4.

	Hierarchy	Level	Triangle Wall Thickness (mm)	Height (mm)	Surface Area (mm^2)
(a)	Fractal	1	14.3324	57.7350	23.5869×10^3
		2	6.4666		
		3	2.0931		
(b)	Hexagram	1	8.1578	57.7350	23.5869×10^3
		2	2.2106		
(c)	H2H3	1	6.6521	57.7350	23.5869×10^3
		2	2.0598		
(d)	H2-only	1	2.0598	57.7350	23.5869×10^3
(e)	H3-only	1	6.6521	57.7350	23.5869×10^3

The presented hierarchical structures, encompassing fractal, hexagram, H2H3, and H2 configurations, exhibit uniform surface area, loading surface area, and volume. These similarities suggest a consistent geometric profile across the various hierarchy levels. The majority of the structures, including fractal, hexagram, and H2H3, demonstrate suitability for 3D printing, as they adhere to essential constraints such as a minimum thickness of 2mm and other printer specifications. However, the H3-only structure stands out as unsuitable for printing due to its excessively high triangle density, violating the critical 2mm thickness constraint.

In the background section, we explore previous research conducted by Qian Cheng to provide context. The methodology outlines the step-by-step approach, including digitalizing curves from Cheng's paper, comparing

results for validation, creating meshes using Gmsh, inputting data into finite element simulations, and analyzing the outcomes. Results and discussion sections present the findings, focusing on key parameter values relevant to energy absorption. Finally, the conclusion summarises the main insights to enhance energy absorption capabilities and suggests potential avenues for further research.

2 Methodology

2.1 Cheng's findings Validation

The methodology commences with the digitisation of curves for HTC-1 and HTC-2. Using the digitised data, we calculated several key performance indexes using formulas provided below to compare our results with those presented in the paper. These indexes are obtained from equations (7) to (11) that characterise cellular composites under in-plane compression.

The nominal stress (σ) and nominal strain (ε) are expressed in terms of compression contact area (S), the height of the structure in compression direction (h), axial compressive force (F), and compression displacement (δ):

$$\sigma = \frac{F}{S} \text{ and } \varepsilon = \frac{\delta}{h} \tag{7}$$

The average stress in the plateau stage (σ_p) is determined using equation (8), where the densification strain (ε_D) is calculated. This equation provides insights into the stress behavior of the material during the plateau region, which is essential for evaluating its mechanical properties:

$$\sigma_p = \frac{1}{\varepsilon_D - \varepsilon_y} \cdot \int_{\varepsilon_D}^{\varepsilon_y} \sigma(\varepsilon) d\varepsilon \tag{8}$$

To compute ε_D, an energy absorption efficiency parameter (η) is introduced:

$$\eta(\varepsilon) = \frac{1}{\sigma(\varepsilon)} \int_0^{\varepsilon} \sigma(\varepsilon)\, d\varepsilon \tag{9}$$

The densification strain (ε_D) represents the strain corresponding to the maximum value of the energy absorption efficiency. It is derived using the energy efficiency method introduced in equation (9) and calculated based on the material's response during compression until densification:

$$\left.\frac{d\eta(\varepsilon)}{d\varepsilon}\right|_{\varepsilon=\varepsilon_D} = 0 \tag{10}$$

Energy absorption (EA) quantifies the total absorbed energy during compression until densification. It is calculated using equation (11), which integrates the instantaneous compressive force (F(z)) with displacement (z) (Zhou et al. 2023). Higher values of EA indicate greater energy absorption capabilities:

$$EA = \int_0^{\delta_D} F(z)\, dz \tag{11}$$

2.2 Mesh Generation and Simulation Input for Analysis

Upon careful examination of the Python code, modifications were implemented to enlarge the initial structures. This Python code, to generate scripts used in Gmsh files, underwent adjustments to enable the creation of larger meshes. By replicating the initial mesh and positioning two identical versions alongside the original, the mesh's width was effectively extended while preserving its height and depth.

Listing 1: Python Code to replicate the initial mesh

```
for i in range(2**nrows):
    Lrow=L/(2.**(nrows+1))
    Hrow=H/(2.**(nrows))
    for j in range(2*2**(nrows+1)-1):
        if-statements to remove the overlapping triangles
```

The Gmsh files generated are subsequently imported into esys-escript. Utilising this finite element software, load compression simulations are conducted, producing data for stress-strain analyses on the structures. To simulate real-world scenarios, compressive loads are uniformly applied from both the top and bottom of the structures simultaneously. Figure 7 illustrates this process, depicting how the compressive load is applied to the structure.

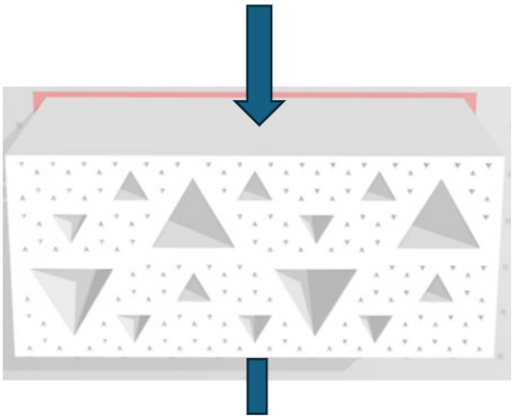

Figure 7: compressive loads are uniformly applied from both the top and bottom of the structures simultaneously.

Through this simulation, we evaluate the mechanical behavior and energy absorption capacities of the structures. Analysis involves scrutinizing stress and strain distributions across our five structures. Key performance indices, notably total energy absorption, are computed to assess their overall energy absorption efficacy.

3 Result and Discussion

The digitised curves, showcased in Figure 6, closely resemble those presented in Cheng's paper (figure 3), displaying an almost identical shape. Utilizing these digitised data, four key performance indices have been

computed and are summarised in Table 3. Upon comparison with the figures from Cheng's paper, our results exhibit a remarkable similarity, further validating his findings.

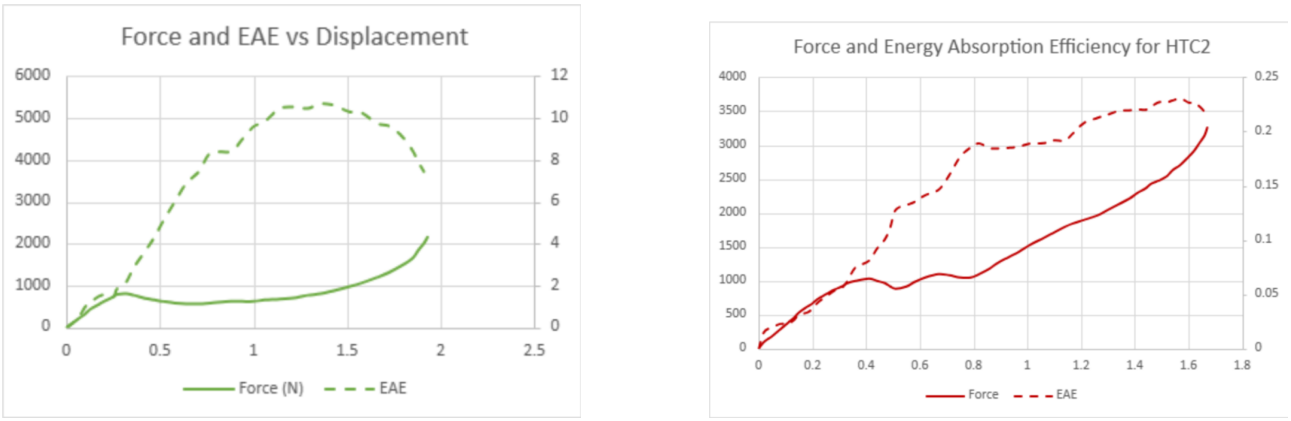

(a) HTC-1 **(b)** HTC-2

Figure 8: Force and Energy Absorption Efficiency (EAE) versus displacement curves plotted by digitalised data

Table 3: Key Performance Metrics for HTC-1 and HTC-2

	Densification Strain	Initial Peak Stress (MPa)	Mean Plateau Stress (MPa)	Total Energy Absorption (J)
HTC-1	0.392	0.661	0.569	8.954
HTC-2	0.459	0.846	1.354	21.892

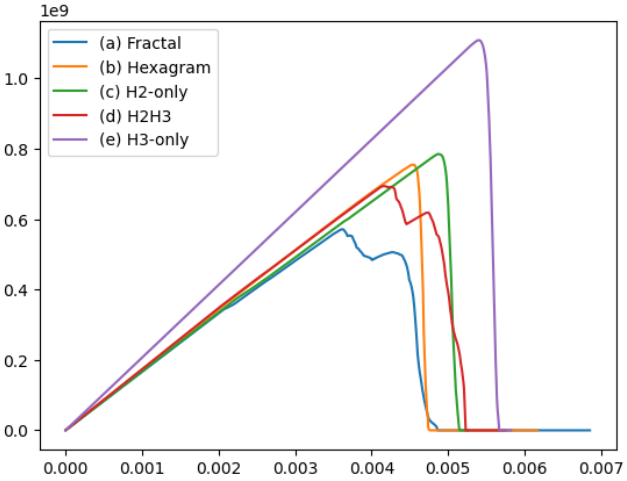

Figure 9: Stress-strain curves to illustrate structures' energy absorption capacity.

For (a) Fractal structure in Figure 9, we observe a two-stage failure mechanism: initially, the larger triangles fail as figure 10, followed by the smaller ones. This sequential failure enhances energy absorption, resulting in

a more gradual response. In contrast, structures such as H2-only and H3-only structures, composed of uniform triangle sizes exhibit abrupt failure, leading to a plateau in their behavior. Sudden failure without warning in brittle materials poses significant risks, particularly in critical structures like bridges. However, by incorporating hierarchy, we introduce two distinct stages of failure, providing a warning sign before complete collapse. This two-stage failure pattern resembles that of ductile materials, enhancing safety and structural integrity.

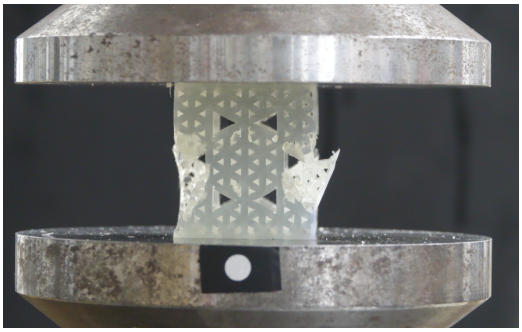

Figure 10: Illustration for a structure with two kinds of triangles typically having the larger triangles falling first.

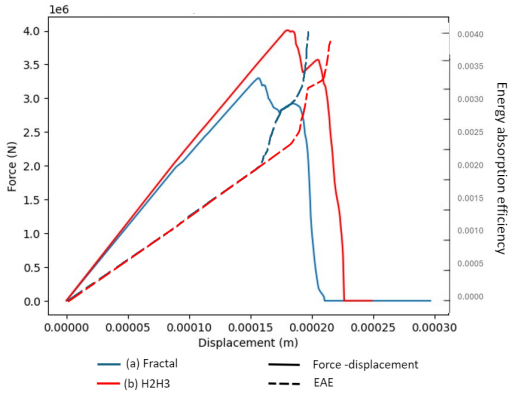

Figure 11: Force-displacement curves (solid lines) and corresponding energy absorption efficiency curves (dashed lines) of Fractal and H2H3 structures to illustrate theirs energy absorption capacity.

The densification strain value of 0.41 cm for Fractal structure illustrates the structure's ability to withstand and deform under applied pressure. Additionally, the total energy absorption capacity of 3.29J before failure provides insights into its ability to withstand impact and deformation. The energy absorption pattern observed in the fractal structure is also evident in the H2H3 regular structure, which features two sizes of triangles: large and small. The H2H3 structure exhibits a densification strain of 0.452 cm and an energy absorption value of 2.796J, which is less than that of the fractal structure.

When examining structures (d) and (e) in Figure 9, which comprise only one size of triangles, the absence of the characteristic stress-strain curve bump indicates a lack of warning signs before collapse. In such instances, the maximum stress that H2 can withstand is approximately 800 MPa, while for H3, it is about 1000 MPa. This indicates that for structures composed of only one type of triangle, an increase in the size of each triangle

results in a decrease in the energy absorption capacity of the structure. Interestingly, the hexagram structure (b) in Figure 9 , despite featuring two types of triangles and having fairly distributed damage, remains brittle. The highest stress and strain values for the hexagram structure are crucial to note. When subjected to a force greater than 700 MPa, the hexagram structure collapses immediately without transitioning through other phases.

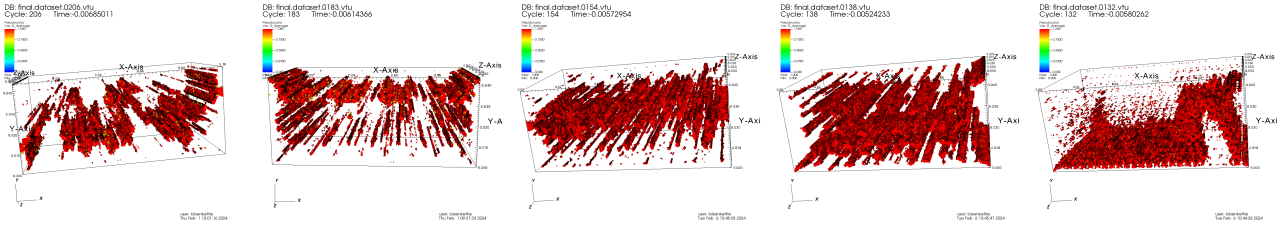

(a) Fractal **(b)** Hexagram **(c)** H2H3 **(d)** H2-only **(e)** H3-only

Figure 12: Damage distribution heatmap when compressive load is applied to each structure

Figure 12 depicts the damage distribution across five structures created by gmsh. Notably, H2 exhibits distributed damage, but Hexagram and H3 show less of it, leading to brittle failure, whereas H2H3 and fractal structures exhibit distributed damage.

Table 4: Key Performance Indexes with experimental compressive loading of ductile materials and numerical simulations of compressive loading of brittle alumina.

	Densification Strain	Initial Peak Stress (MPa)	Total Energy Absorption (J)
Ductile materials			
HTC-1	0.395	0.572	8.611
HTC-2	0.460	1.208	21.211
Brittle alumina			
Fractal	0.410	0.570	3.290
H2H3	0.452	0.685	2.796

To gain deeper insights, these results were compared with Cheng et al.'s findings, which focused on materials exhibiting greater ductility. While Cheng utilised thermoplastic urethane, known for its ductile properties, I employed ceramic material in my research. This discrepancy contributes to the observation that my structures absorb less energy than theirs.

Furthermore, while Cheng compared fractal structures with larger H1 and H2 configurations, my research specifically compares H2 and H3 structures using brittle ceramic material. This distinction underscores the variations in material properties and structural configurations between the two studies.

4 Conclusion

In conclusion, this study investigated the mechanical behavior and energy absorption capabilities of hierarchical structures, specifically focusing on ceramic materials. By analyzing stress-strain curves and key performance metrics such as densification strain and energy absorption, we gained valuable insights into the structural response under quasi-static compression. One notable finding is the introduction of hierarchy in structural design, which enhances ductility and provides warning signs before complete collapse. Unlike regular structures, hierarchical configurations exhibit a two-stage failure mechanism, indicating improved structural integrity and safety. These findings underscore the significance of hierarchy in enhancing the mechanical performance of materials, offering potential applications in diverse fields such as protective gear and structural engineering. Moreover, we were surprised by the results for the hexagram Sierpinski triangles, which did not exhibit a two-step failure process as expected. Additionally, for structures that consist of only one kind of triangles, as the size of each triangle increases, the energy absorption capacity of the structure and the yield strength decreases. Moving forward, further research can explore optimisation strategies to maximise the ductility and energy absorption efficiency of hierarchical structures, thus advancing their utility in real-world applications.

5 Acknowledgement

I extend my special thanks to Dr. Louise Olsen-Kettle for her invaluable supervision and guidance throughout this project. Gratitude to Jia Hui Li for his assistance in the crucial task of printing the structures. I appreciate Nathan Clisby for providing me with the opportunity through the scholarship and introducing me to this impactful project. My sincere thanks to AMSI for organizing the event and supporting this project.

6 Statement of Authorship

- Minh Thu Nguyen: Digitised curves, extended python code, generated Gmsh files, computed key performance indexes, wrote the paper, and analyzed the results.
- Dr. Louise Olsen-Kettle: Supervised the project, provided input on project direction, supplied the initial Python code, conducted simulations, assisted in result interpretation, and proofread this report.
- Jia Hui Li: Printed the structures used in the experiments.

References

Cheng, Q., Yin, J., Wen, J. & Yu, D. (2023), 'Mechanical properties of 3d-printed hierarchical structures based on sierpinski triangles', *International Journal of Mechanical Sciences* **247**, 108172.
URL: *https://www.sciencedirect.com/science/article/pii/S0020740323000747*

Daneshvar, D. H., Baugh, C. M., Nowinski, C. J., McKee, A. C., Stern, R. A. & Cantu, R. C. (2011), 'Helmets and mouth guards: The role of personal equipment in preventing sport-related concussions', *Clin Sports Med* **30**(1), 145–163.

F. P. Bos, E. B. & Salet, T. A. M. (2019), 'Ductility of 3d printed concrete reinforced with short straight steel fibers', *Virtual and Physical Prototyping* **14**(2), 160–174.
URL: *https://doi.org/10.1080/17452759.2018.1548069*

Fernandes, F. A. O., de Sousa, R. J. A., Ptak, M. & Migueis, G. (2019), 'Helmet design based on the optimization of biocomposite energy-absorbing liners under multi-impact loading', *Appl. Sci.* **9**(4), 735. Author to whom correspondence should be addressed.
URL: *https://doi.org/10.3390/app9040735*

Geuzaine, C. & Remacle, J.-F. (2009), 'Gmsh: A 3-D finite element mesh generator with built-in pre- and post-processing facilities', *International Journal for Numerical Methods in Engineering* **79**(5), 561–582.
URL: *https://doi.org/10.1002/nme.2579*

Gross, L., Bourgouin, L., Hale, A. & Mühlhaus, H.-B. (2007), 'Interface modeling in incompressible media using level sets in escript', *Physics of the Earth and Planetary Interiors* **163**(1-4), 23–34.

Lu, G. (2003), *Energy Absorption of Structures and Materials*, Woodhead Publishing, Cambridge, UK. Cited by 1542.

Mondal, S. (2019), Numerical modelling of damage evolution and fracture propagation in brittle materials, PhD thesis, School of Earth and Environmental Sciences, The University of Queensland.

Mondal, S., Olsen-Kettle, L. & Gross, L. (2019), 'Simulating damage evolution and fracture propagation in sandstone containing a preexisting 3-d surface flaw under uniaxial compression', *International Journal for Numerical and Analytical Methods in Geomechanics* **43**(7), 1448–1466.

Mondal, S., Olsen-Kettle, L. & Gross, L. (2020*a*), 'Regularization of continuum damage mechanics models for 3-d brittle materials using implicit gradient enhancement', *Computers and Geotechnics* **122**, 103505.

Mondal, S., Olsen-Kettle, L. & Gross, L. (2020*b*), 'Sensitivity of the damage response and fracture path to material heterogeneity present in a sandstone specimen containing a pre-existing 3-d surface flaw under uniaxial loading', *Computers and Geotechnics* **126**, 103728.

Olsen-Kettle, L., Mondal, S. & Tsang, H.-H. (2022), 'Damage delocalisation in skeletal muscle-inspired hierarchical armoured structures for impact protection', *Composite Structures* . Received 9 February 2022, Revised 24 May 2022, Accepted 18 June 2022, Available online 22 June 2022, Version of Record 29 June 2022.
URL: *https://doi.org/10.1016/j.compstruct.2022.115947*

Peerlings, R. H., Brekelmans, W., De Borst, R. & Geers, M. G. (2000), 'Gradient-enhanced damage modelling of high-cycle fatigue', *International Journal for Numerical Methods in Engineering* **49**(12), 1547–1569.

Schaa, R., Gross, L. & du Plessis, J. (2016), 'Pde-based geophysical modelling using finite elements: examples from 3d resistivity and 2d magnetotellurics', *Journal of Geophysics and Engineering* **13**(2), S59–S73.

Taylor, D. (2018), 'Measuring fracture toughness in biological materials', *Journal of the Mechanical Behavior of Biomedical Materials* **77**, 776–782.
URL: *https://www.sciencedirect.com/science/article/pii/S1751616117302953*

Velling, A. (2020), 'Stress-strain curve'. Accessed on 26/02/2024.
URL: *https://fractory.com/stress-strain-curve/*

Wang, J., Yang, B., Lin, X., Gao, L., Liu, T., Lu, Y. & Wang, R. (2020), 'Research of TPU materials for 3D printing aiming at non-pneumatic tires by FDM method', *Polymers* **12**(11), 2492.
URL: *https://doi.org/10.3390/polym12112492*

Zhou, J., Liu, H., Dear, J. P., Falzon, B. G. & Kazancı, Z. (2023), 'Comparison of different quasi-static loading conditions of additively manufactured composite hexagonal and auxetic cellular structures', *International Journal of Mechanical Sciences* **244**, 108054.
URL: *https://www.sciencedirect.com/science/article/pii/S0020740322009328*